Modelling of R/C members accounting for shear failure localisation: Hysteretic shear model

Dimitrios K. Zimos[a], Panagiotis E. Mergos[a] and Andreas J. Kappos[a,b]

[a]*Research Centre for Civil Engineering Structures, Civil Engineering Department, City, University of London, London, EC1V 0HB, United Kingdom*

[b] *Civil Engineering Department, Aristotle University of Thessaloniki, Thessaloniki, GR 54124*

SUMMARY

Reinforced concrete (R/C) frame buildings designed according to older seismic codes represent a large part of the existing building stock worldwide. Their structural elements are often vulnerable to shear or flexure-shear failure, which can eventually lead to loss of axial load resistance of vertical elements and initiate vertical progressive collapse of a building. In this study, a hysteretic model capturing the local shear response of shear-deficient R/C elements is described in detail, with emphasis on post-peak behaviour; it differs from existing models in that it considers the localisation of shear strains after the onset of shear failure in a critical length defined by the diagonal failure planes. Additionally, an effort is made to improve the state of the art in post-peak shear response modelling, by compiling the largest database of experimental results for shear and flexure-shear critical R/C columns cycled well beyond the onset of shear failure and/or up to the onset of axial failure, and developing empirical relationships for the key parameters defining the local backbone post-peak shear response of such elements. The implementation of the derived local hysteretic shear model in a computationally efficient beam-column finite element model with distributed shear flexibility, which accounts for all deformation types, will be presented in a forthcoming paper.

Keywords: Reinforced concrete structures; Substandard members; Hysteresis model; Shear response; Post-peak response; Axial failure

1. INTRODUCTION

Reinforced concrete buildings designed according to older seismic codes (or even without adhering to any code) represent a large part of the existing building stock worldwide. Transverse reinforcement in their structural elements is typically inadequate, widely spaced or poorly anchored, rendering them vulnerable to shear failure subsequent, or even prior, to yielding of their longitudinal reinforcement. Shear failure can eventually lead to loss of axial load capacity of vertical elements, through disintegration of the poorly confined concrete core and the consequent axial load capacity decrease [1], and initiate vertical progressive collapse of a building. This collapse type has been shown through post-earthquake reconnaissance to be the most common reason for R/C frame building collapse [2]. Thus, it is important to be capable of accurately and efficiently assessing the response of shear-deficient R/C members to earthquake-induced actions, in order to evaluate their vulnerability and decide on necessary measures to be taken, such as implementing a retrofit scheme to increase their resistance.

Modelling of an R/C member under lateral loading should consider all three components of deformation , i.e. flexural, anchorage slip and shear [3]. The former can be captured quite accurately by the available finite element models providing an accurate prediction of the hysteretic response of code-conforming members. Nevertheless, the other two deformation components readily become significant, when dealing with sub-standard members. It has been observed experimentally that in plastic hinge regions, shear strength decreases [4], [5] and shear deformations increase considerably, despite the fact that shear demand remains practically constant [3]. This impacts the response of flexure-shear critical members that fail in shear after experiencing flexural yielding. Several models have been developed to predict the maximum shear strength of a member and its degradation with ductility demand, accounting for the aforementioned interaction. Amongst them are the model by

Priestley *et al*. [6], Sezen & Moehle's model [7] and a more recent one based on statistical analysis of a large number of tests of flexure-shear critical column specimens, by Biskinis *et al*. [8].

Tests on R/C members subjected to seismic loading are traditionally terminated shortly after the onset of shear failure, not shedding much light on their post-peak response. Nonetheless, there has been a recent shift of interest during the last two decades, producing a sizeable amount of data regarding the post-peak response of R/C elements, including the onset of their axial collapse. Some noteworthy experimental works are those by Moehle *et al*. (e.g. [1]) , Ousalem *et al*. (e.g. [9], [10]) and Yoshimura *et al*. (e.g. [11]).

It has been experimentally observed (e.g. [12]–[14]) that deformations after the onset of shear failure tend to concentrate at a specific shear-damaged member region; in essence, this mainly corresponds to the relative rigid body displacement between the separated upper and lower parts of the column along the diagonal shear failure crack.

Advanced, structural mechanics based, shear models like the Modified Compression Field Theory (e.g. [15]) or the softened truss and membrane models ([16], [17]), have proven to be rather accurate, but are limited to pre-peak shear behaviour. More recently, the Axial-Shear-Flexure Interaction approach was proposed [18], also considering the post-peak shear response. Nonetheless, these approaches involve high computational demand and do not capture the hysteretic response of R/C elements, hence do not readily lend themselves to use in seismic analysis of complex R/C structures.

In the last two decades, there have been several *macro-models* aiming at modelling the cyclic lateral behaviour of sub-standard R/C elements, taking into account shear deformations and anchorage slip rotations (e.g. [3], [19]–[23]). Some of them also extend into the post-peak domain of the response, even predicting the onset of axial failure of an element, i.e. the point where axial capacity reaches axial demand; after this point, axial shortening increases with simultaneous decrease of axial load capacity. This is a critical point in assessing the behaviour of an existing structure, especially when it comes to predicting the initiation and cascade of progressive collapse. These macro-models offer reasonable predictions of sub-standard R/C member response, but they often lack accuracy in the post-peak range, largely owing to the scarcity of experimental tests of specimens up to the onset of axial failure. For example, post-peak response has often been determined by the onset of shear failure and the onset of axial failure (e.g. [24], [25]), assuming that shear strength is completely lost at the latter point. However, there is experimental evidence that shear strength is not always zero at the onset of axial failure (e.g. [26]). Other studies (e.g. [19], [23]) assume that residual strength develops after shear failure without solid support by experimental evidence. These issues will be addressed later in this paper. Additionally, all these beam-column models are based on inter-storey drift ratios, despite the aforementioned observation that localised drift ratios at the shear-damaged regions are more representative of the actual response, since shear deformations tend to concentrate there after the onset of shear failure.

In this study, a local hysteretic shear model is proposed. Its main conceptual novelty lies in the consideration of the afore-described localisation of shear strains in the shear-damaged region after the onset of shear failure. Additionally, it is attempted to advance the state of the art in shear response modelling one step further, by compiling a database of experimental results of shear and flexure-shear critical R/C columns - the largest of its kind -, investigating their post-peak response through statistical analysis and developing empirical relations for key parameters defining the local post-peak response of such elements. The hysteretic shear model will be incorporated into a computationally efficient member-type model for the full-range response of substandard R/C elements in a forthcoming paper[*], with a view to accurately capturing the hysteretic response of shear-deficient members and structures. It is a flexibility-based, spread-inelasticity, phenomenological model, based on local deformations

[*] Zimos, D.K., Mergos, P.E. and Kappos, A.J., Modelling of R/C members accounting for shear failure localisation: Finite element model and verification, to be submitted to EESD, 2017.

rather than inter-storey displacement, hence more objectively accounting for the interaction of inelastic flexural and shear deformations at a local level, including the gradual decrease of an element's shear resistance, and more reliably predicting the location and extent of shear deformations, without relying on assumptions about the bending moment distribution.

2. HYSTERETIC SHEAR MODEL DESCRIPTION

The hysteretic shear model is formulated in terms of shear force V against shear distortion γ at section level and comprises of the V-γ backbone curve and the hysteresis rules determining the response under cyclic loading. Its initial V-γ backbone curve is defined disregarding interaction with flexure and can be used for elements that have not yielded in flexure, as well as for the elastic regions of members that have developed flexural yielding (Figure 1). This curve is defined by the shear cracking point where the nominal tensile principal stress exceeds the tensile concrete strength (γ_{cr}, V_{cr}), the onset of yielding of the transverse reinforcement, where the maximum shear strength is attained (V_{max}, γ_{st}), and a plateau, where shear strains increase up to the onset of initiation of lateral strength degradation, i.e. the onset of shear failure ($\gamma_{sh,f}$, V_{max}).

Subsequently, a bi-linear descending branch is followed up to the onset of axial failure, having a breaking point at half the maximum strength and defined by the slopes of the two linear segments $S_{pp,1}\times V_{max}$ and $S_{pp,2}\times V_{max}$ respectively (Figure 1). This shape is chosen herein due to its simplicity and satisfactory correlation with the recorded experimental post-peak responses demonstrated in the next section. Furthermore, it can readily be converted to a linear descending branch by setting the slope of the second branch equal to the slope of the first.

The descending branch is terminated at the point of onset of axial failure, where physical collapse of the member takes place. The definition of the onset of axial failure in this study is both deformation-based and force-based. More specifically, a column is considered to have failed axially (i.e. lost its bearing capacity), if the shear deformation limit corresponding to the onset of axial failure has been reached. This deformation limit is equal to $\gamma_{sh,f}$ plus the post-peak shear distortion up to the onset of axial failure $\gamma_{t,pp}$ (Figure 1). However, if shear strength degrades to zero before this critical deformation is reached, the onset of axial failure is specified by the point where the descending branch meets the axis of shear deformations (i.e. point on the descending branch with zero shear strength).

The initial V-γ curve is modified in plastic hinge regions to account for shear-flexure interaction. This is based on the current curvature ductility demand and the ensuing degradation of the "concrete contribution" to shear strength, resulting in an increase of the truss contribution. The parts of the backbone curve between the shear strength corresponding to flexural yielding (γ_y, V_y in Figure 1) and the onset of shear failure are affected to consider shear-flexure interaction (more details given in [3]).

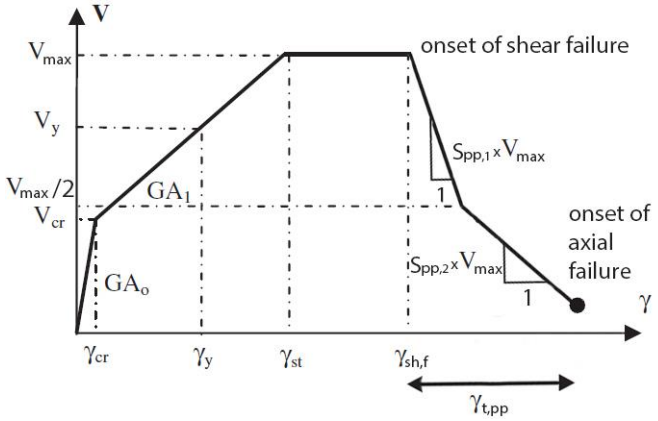

Figure 1: V-γ primary curve of the proposed shear model (without shear-flexure interaction).

After the onset of shear failure, the assumption adopted in this study is that flexural and slip-induced deformations do not increase further than their values at peak strength, i.e. the entire post-

peak displacement is attributed to shear deformations. This assumption has also been adopted in other similar models (e.g. [24], [25]) and is supported by experimental evidence (e.g. [27]).

Furthermore, it has been previously established based on experimental observations (e.g. [12]–[14]) that deformations after the onset of shear failure tend to concentrate in a specific member length, called *critical shear length*, defined by the diagonal failure planes; the clear length of a column, L_{cl}, the critical shear length, L_{cr}, and the shear failure plane angle or herein termed *critical shear crack angle*, θ_{sh}, are illustrated in Figure 2. The localisation of post-peak shear strains in the critical length is herein termed *shear failure localisation*. In essence, it mainly represents the relative rigid body displacement between the discrete upper and lower parts of the column along the shear crack; this can be seen in the image of an actual experimental test of a shear-deficient R/C column in Figure 2 [28].

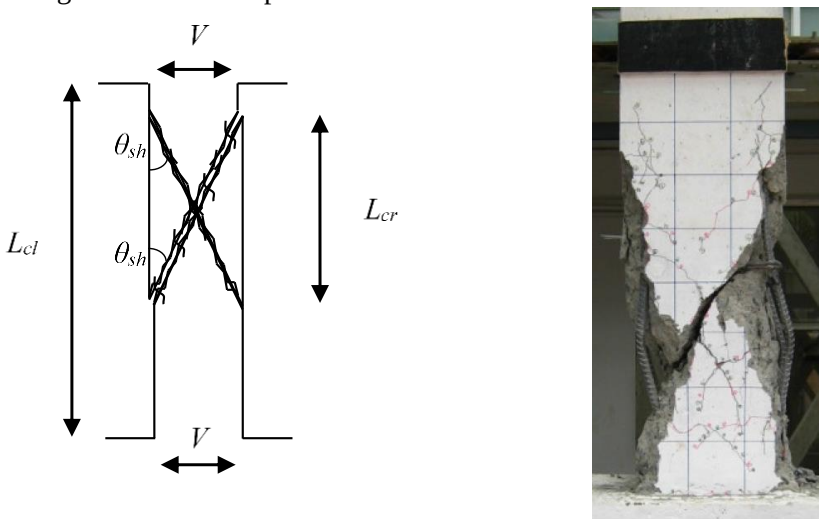

Figure 2: Illustrative sketch of the critical length in a shear-damaged column (a). Image of an actual experimental test of an axially failed shear-deficient R/C column (b) [28].

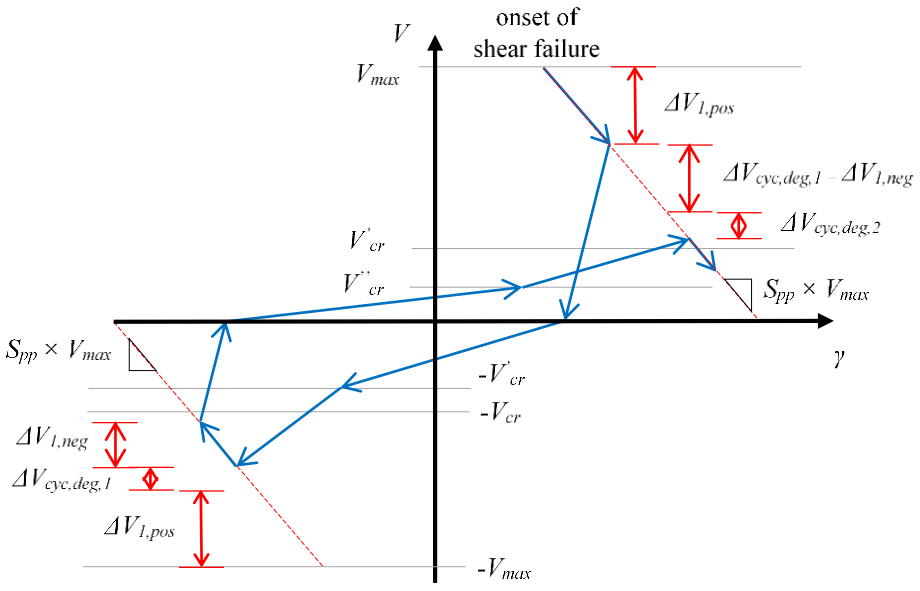

Figure 3: Hysteresis rules after the onset of shear failure.

Following this approach, after the onset of shear failure, shear deformations will be expressed as:

$$\gamma = \gamma_{sh,f} + \frac{\delta_{pp}}{L_{cr}} = \gamma_{sh,f} + \frac{\delta_{pp}}{h \cot \theta_{sh}} \quad (1)$$

where γ is the average shear strain in the critical shear length; $\gamma_{sh,f}$ is the shear strain at the onset of shear failure in the critical shear length; δ_{pp} is the post-peak lateral displacement; h is the height of the section.

The hysteresis rules adopted in the pre-peak domain of the shear model are based on those of Ozcebe & Saatcioglu [4], with several improvements (presented elsewhere [3], [29]) for numerical stability in dynamic analysis, as done by other researchers in similar models [20]. Pinching, unloading and reloading stiffness deterioration, as well as cyclic strength degradation, are all accounted for.

In the post-peak domain, the same hysteresis rules are generally applied [3], [4], [29]; however, some modifications are proposed here, to make them compatible with the response of specimens after the onset of shear failure, as shown in Figure 3 (showing the linear descending branch case, for the sake of simplicity; $\Delta V_{1,pos}$ and $\Delta V_{1,neg}$ denoting in-cycle strength degradation in the positive or negative direction, respectively; $\Delta V_{cyc,deg,i}$ (i=1,2) denoting cyclic strength degradation). In-cycle strength degradation follows the aforementioned backbone descending branch(es), for instance $S_{pp} \times V_{max}$ in Figure 3. Post-peak cyclic degradation is accounted for as in [4], in line with the calibration of the post-peak descending branch (section 3.3), i.e. the end reloading point lies on the descending branch (Figure 3) and, subsequently, the response follows the defined descending branch slope(s). Pinching and reloading stiffness deterioration are accounted for using a bilinear reloading curve as in the pre-peak domain [4], [29]. Nonetheless, the shear cracking strength, V_{cr}, which is the ordinate of the end point of the first reloading branch, degrades, unlike the pre-peak domain. Its degradation is proportional to the degradation of the end point of the second reloading branch (e.g. V_{cr} and V'_{cr} in proportion to V_{max} and $V_{max} - \Delta V_{1,pos} - \Delta V_{cyc,deg,1}$ in Figure 3). Were it not degrading, an end point of the second reloading branch with strength lower than the shear cracking strength would inevitably appear, leading to a negative stiffness of the second reloading branch. Unloading follows a linear branch with the same stiffness deterioration rules as in the pre-peak domain [29]. Shear strength degradation mirroring is also taken into account; this effectively means that once a certain amount of strength is lost in one loading direction, a higher strength cannot be reached in the other. For example, in Figure 3, the descent starts from the onset of shear failure with V_{max} on the positive side, followed by $\Delta V_{1,pos}$ in-cycle degradation. The strength of the vertex point on the negative direction becomes $-(V_{max} - \Delta V_{1,pos} - \Delta V_{cyc,deg,1})$. Similarly, the in-cycle degradation on the negative side ($\Delta V_{1,neg}$) is subtracted from the positive vertex point strength upon reloading on the positive side for the first time, and so forth. This assumption has been adopted in other similar models (e.g. [23]) and is supported by experimental evidence (e.g. [12], [1]).

3. CALIBRATION OF HYSTERETIC SHEAR MODEL PARAMETERS IN THE CRITICAL SHEAR LENGTH

The necessary parameters for the up-to-peak backbone curve have been presented in detail elsewhere [3].The key parameters that have to be defined to model the local post-peak shear response of an R/C element are the critical length of the shear-damaged region, hence the angle of the shear failure plane, the descending branch slopes after the onset of shear failure and the shear deformation at the onset of axial failure.

Although a mechanics-based approach would in principle be preferable to obtain such parameters, it is currently not feasible considering the inherent uncertainty of the post-peak cyclic shear response, with a considerable effect of deformation history and experimental setup that usually cannot be accounted for, as well as the randomness of the succession of degrading phenomena taking place at a lower level. This fact is corroborated by the high variability in the results of similar models for the post-peak response of shear-deficient R/C elements (e.g. [30]) and the considerable variability produced (of the order of 30-50%) even for pre-peak parameters of R/C elements, even when employing very extensive databases [31]. Additionally, it is also corroborated by the adoption of empirical models even for the pre-peak response of existing structures in Eurocode EN1998-3 [31],

[32] and, lastly, by the fact that even when trying to develop a mechanics-based model, shear deformations might need to be accounted for through an empirical correction factor [33].

3.1 Database compilation

A large database of shear and flexure-shear critical elements, which were cycled well beyond the onset of shear failure or which had clear photographic evidence of their shear cracking, was compiled. It comprises 151 rectangular R/C columns, 68 of which have sustained flexure-shear failure and 83 shear failure prior to flexural yielding. To the best of the authors' knowledge, it includes the largest collection of rectangular R/C columns cycled well into the post-peak domain after the onset of shear failure (116) and/or eventually failing axially (89). Their characteristics in terms of longitudinal reinforcement ratio (ρ_l), transverse reinforcement ratio (ρ_w), stirrup spacing over effective depth (s/d), aspect ratio (L_s/d), maximum shear stress ratio ($\tau_{max}/\sqrt{f_c}$) and axial load ratio (v) (3 specimens in tension are presented separately) are summarised in Table 1. More details on the specimens of the database and their characteristics can be found in [34].

Table 1: Main specimen characteristics of the database.

	Min	**Mean**	**Max**
ρ_l **(%)**	0.16	2.25	4.76
ρ_w **(%)**	0.08	0.38	1.59
s/d	0.11	0.44	2.52
L_s/d	0.90	1.94	4.29
$\tau_{max} / \sqrt{f_c}$	0.22	0.57	1.23
v **(compressive)**	0.00	0.27	0.80
v **(tensile)**	-0.26	-0.15	-0.07

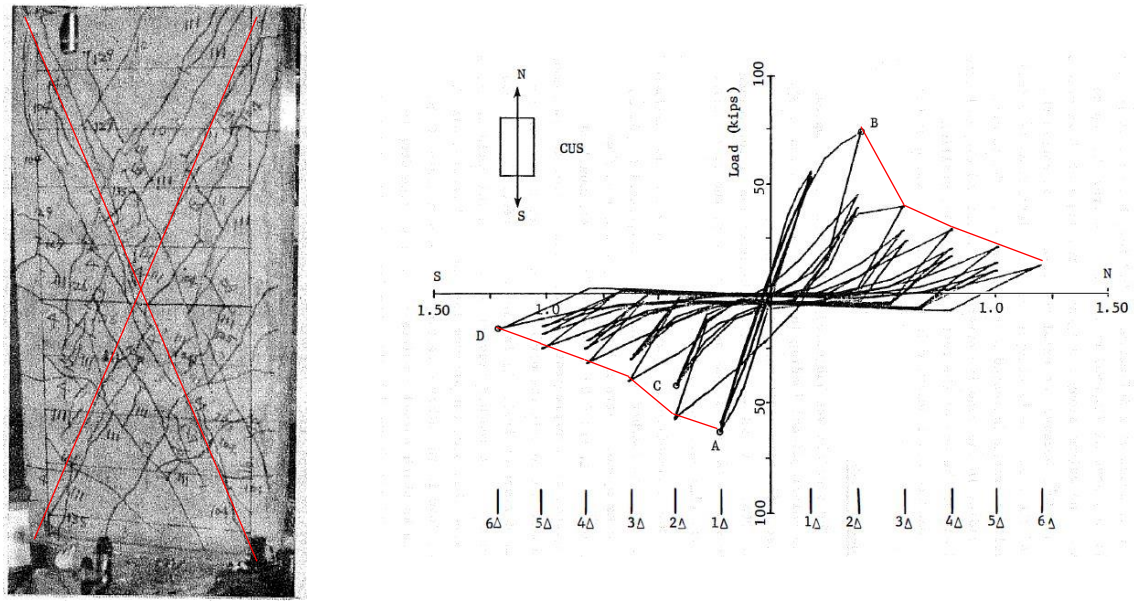

(a) (b)

Figure 4: Indicative extraction of critical shear crack angle (a) and descending branch curve (b) from experimental data [35].

The values of the inclined shear failure plane angle, herein termed "critical shear crack angle", were obtained from available photographic documentation of specimens exceeding the onset of shear failure (for example, Figure 4a). It is noted that this angle does not correspond to the first shear cracks that appear on a specimen along the principal compressive stress trajectories, when the tensile strength of concrete is reached. These can be readily calculated according to structural mechanics principles

and generally result in steeper angles than the experimentally observed ones [13]. The critical shear crack angle corresponds to an idealised inclined failure plane, which forms at shear failure, and is herein measured with respect to the longitudinal axis of the member. In shear critical specimens, either the major shear crack - if there was a clear one -, or the average inclination of the shear cracks was taken into account (e.g. Figure 4a). In the case of flexure-shear critical members with a fan-shaped crack pattern at the end-region, the steepest one (smallest angle) was taken into account - being considered equivalent to the inclination of the crack that would form in the intermediate region without prior development of flexural hinges [36] -, disregarding potential horizontal parts at the end due to flexural cracking. Furthermore, cracks parallel to the longitudinal axis were disregarded (in the average calculation), as they are usually caused by bond-split of the longitudinal reinforcement. In most cyclic tests, shear cracks appear in both directions with the characteristic X-pattern (e.g. Figure 4a); in these cases the average of both directions is used. All the double-curvature experiments, as well as flexure-shear critical cantilever ones, were taken into account, since the few shear critical cantilever ones were observed to develop higher angle values due to corner-to-corner cracking, which might not be representative of an actual building column. Corrections were applied to account for the rotation of the specimen with regard to the direction of the photograph and the downward or upward perspective.

Only specimens with at least 30% strength degradation were considered, in order to have a genuine descending branch response. Thus, traditional experiments performed up to 15% or 20% strength degradation, which constituted the overwhelming majority until recently, were excluded. The descending branch curve was obtained by the peaks of the first cycles at each displacement level of the post-peak domain (e.g. Figure 4b) as well as potential parts of in-cycle strength degradation of these first cycles, starting off from the point of maximum strength of the respective direction of the response (i.e. points B and A in Figure 4b). In the cases where shear strength degrades below zero, the intersection of the response with the zero-strength line is recorded as the displacement at the onset of axial failure. Otherwise, the maximum displacement developed by the specimen is conventionally defined as the one at onset of axial failure, although in some cases the actual onset of axial failure takes place during a load reversal.

3.2 Critical shear crack angle

The critical shear crack angle has often been assumed independent of column properties (e.g. 45^o) in the process of developing a shear or axial resistance model (e.g. [6], [13]). As this angle affects (through L_{cr}) the modelling of the post-peak part of the shear force vs deformation curve, a realistic estimate of its value would be worthwhile, hence an appropriate expression for this angle was sought. There were 54 shear (S) and 34 flexure-shear critical (FS) specimens of the database, for which there was adequate data available to obtain the critical shear crack angle.

Existing shear crack angle models were tested against the experimentally measured values, to select an appropriate one to use in the context of the current model [37]. Nevertheless, none was found to provide accurate estimates of the observed angles and account for all the influential parameters. Subsequently, correlations of this angle with design variables were investigated. Based on this dataset, several patterns emerged, the most important of which are presented here (Figure 5):

- In line with structural mechanics principles, increasing axial load ratio (v) tends to decrease the shear crack angle, since the trajectories of the principal compressive stresses - along which the first shear cracks will form – are oriented closer to the longitudinal axis of the member.
- Transverse reinforcement ratio (ρ_w) is shown to have a positive correlation with the angle, although transverse reinforcement has hardly any influence on the principal stress trajectories prior to shear cracking, hence on the initial crack inclination. However, the angle of interest in the present model apparently includes the propagation of shear crack at varying angles, the angle change being significantly affected by the yielding transverse reinforcement.
- Longitudinal reinforcement ratio (ρ_l) seems to play no role whatsoever in either case (S or FS).

This is consistent with the mechanics of shear cracking, but contradicts previous studies (e.g. [36]) that have considered it an important parameter.

- Aspect ratio (L_s/d) has a strong negative correlation in the case of shear critical elements, as expected, because of the influence on the trajectories of the principal compressive stresses. In flexure-shear critical elements, however, it has a slightly positive correlation, which is not in line with the previous observation. Although the first shear cracks form similarly to what was described for shear critical elements, the shear strains subsequently concentrate in the end-regions, where flexural yielding has already taken place. As the shear span (M/V) increases, the influence of flexure over shear becomes more pronounced, which probably leads to even "flatter" idealised critical shear crack angles, closer to the horizontal flexural cracks.
- In general, FS members seem to have higher values of shear crack angle, the crack being confined in the end-region of the member that has yielded. Other important parameters that influence the shear crack angle, like cross-section shape and loading conditions, were beyond the scope of the current investigation, which was based on a database of only square/rectangular specimens and included mostly a double-curvature loading condition with forces acting at the ends of the members.

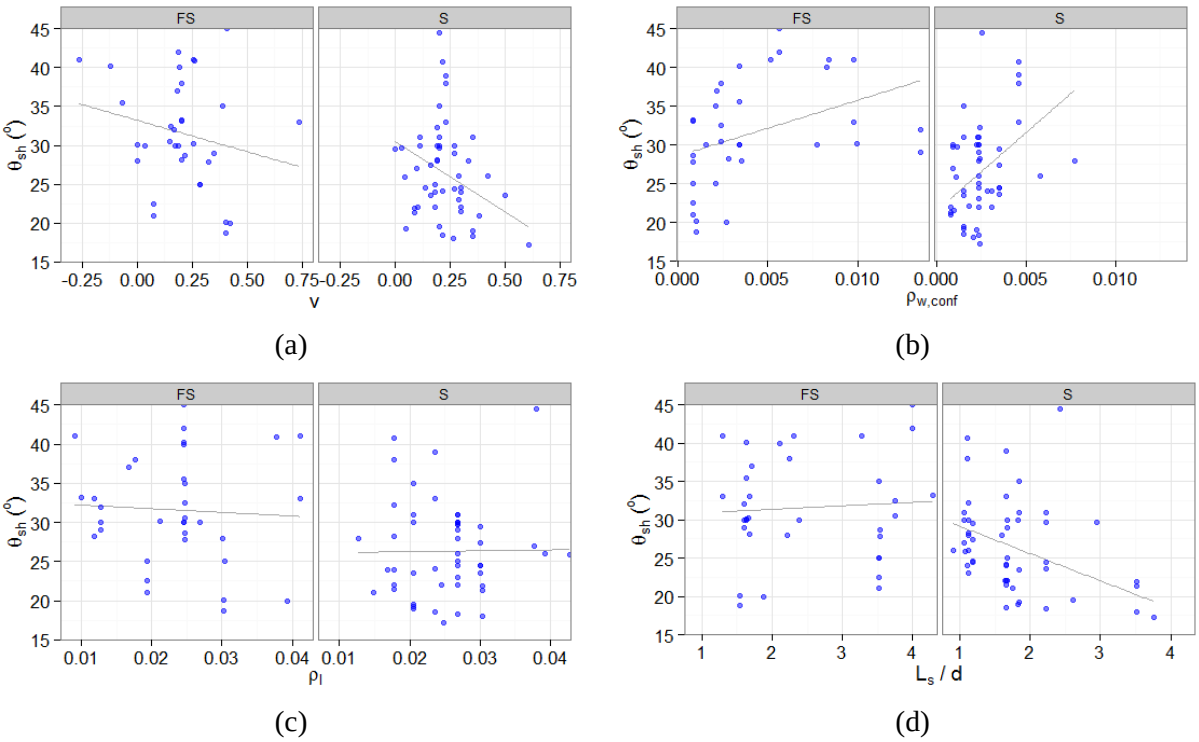

Figure 5: Correlation of the measured shear crack angle with axial load ratio (a), transverse reinforcement ratio (b), longitudinal reinforcement ratio (c), aspect ratio (d), divided into shear (S) and flexure-shear (FS) critical specimens.

Based on the aforementioned trends and significance tests of the predictor variables, various empirical relationships were explored. Through a step-wise predictor variable elimination procedure, 10-fold-cross-validation [38] and optimisation using the Levenberg-Marquardt nonlinear least-squares algorithm (e.g. [39]), the best model developed was the following:

$$\theta_{\min} = \tan^{-1}\frac{h}{L_{cl}} < \theta_{sh} = 165\frac{\beta \times \rho_{w,conf}^{0.0397}}{(v+2.6)^{0.33}} - 66.3 < \theta_{\max} = 45^{o} \quad (2)$$

where h is the height of the cross-section; L_{cl} is the clear length of the member; β is a parameter that differentiates between shear and flexure-shear critical members, equal to 1.00 for S and 1.06 for FS elements; $\rho_{w,conf}$ is the transverse reinforcement ratio normalised to the confined concrete area (stirrup spacing multiplied by the confined section width), introduced with its actual value (not in %); v is the

axial load ratio. The minimum value is a geometrical limitation of the shear crack applying to columns with a very low aspect ratio, as also explained by Elwood & Moehle [13]. Were this limit not imposed, the angle could be lower than the angle of the diagonal connecting the two ends of the column (corner-to-corner crack), essentially leading to an L_{cr} higher than the length of the column itself.

Eq. 2 yields a mean experimental-to-predicted value of 1.00, a median of 0.98 and a *CoV* of 21.9% (Figure 6). It applies to specimens in the following range of parameters: $-0.26 \leq v < 0.75$, $0.08 < \rho_{w,conf} \leq 1.35$ (%), $0.91 \leq \rho_l < 4.28$ (%), $330 < f_{yl} \leq 700$ (MPa), $270 \leq f_{yw} \leq 587$ (MPa), $13.5 \leq f_c \leq 86$ (MPa), $0.9 < L_s/d < 4.3$, where f_{yl} and f_{yw} are the yield strengths of the longitudinal and transverse reinforcement and f_c represents the concrete compressive strength. Figure 7 shows the values of the critical shear crack angle that Eq. 2 would result in, across the whole range of the relevant parameters, i.e. axial load and transverse reinforcement ratios, for shear and flexure-shear critical specimens. For values of parameters representative of common structures (i.e. $0.2 \leq v \leq 0.3$ and $0.2 \leq \rho_w \leq 0.6$ (%)), angles of approximately 25º-30º and 30º-35º would be expected for S and FS specimens, respectively.

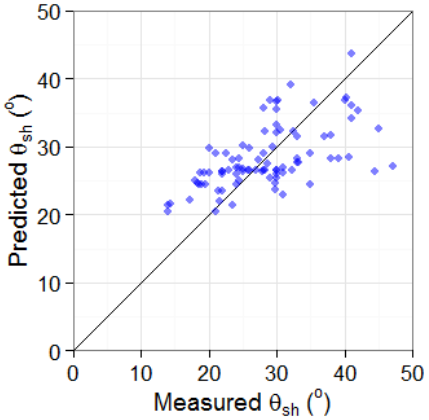

Figure 6: Shear crack angles measured experimentally against the ones predicted by Eq. 2.

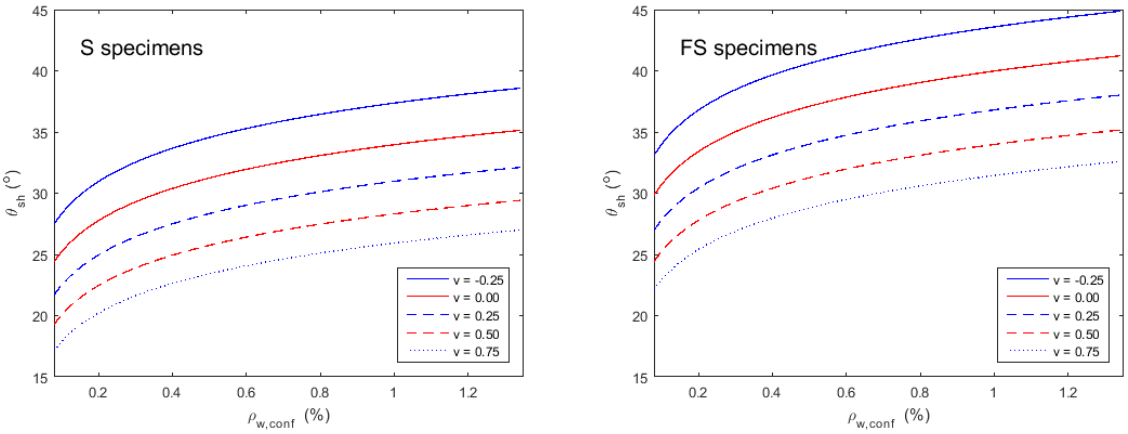

Figure 7: Critical shear crack angle predicted by Eq. 2 along the range of potential axial load and transverse reinforcement ratios (normalised to confined concrete area), for shear (a) and flexure-shear critical specimens (b).

3.3 Descending branch

Shear failure initiation taking place in one direction was hypothesised to influence behaviour in the other direction, so the overall relation between the slopes of the descending branches in either direction was investigated more closely. According to the boxplot in Figure 8a, it seems that the difference is not really significant, with the majority of specimens ranging between 0.9 and 1.3, i.e. having approximately equal slopes in both directions. Therefore, the average of the response in the

two directions was used to calculate the descending branch slope for each specimen.

The shape of the post-peak descending branch has been investigated using the specimens in the database. Initially a non-linear branch was sought, which would be able to represent both concave and convex degradation curves. The relationship that was assumed was the following:

$$\frac{V}{V_{\max}} = 1 - a \times (\gamma - \gamma_{sh,f})^{c} \quad (3)$$

where V_{max} is the maximum shear strength that occurs at the onset of shear failure, $V \leq V_{max}$ the strength at any loading level after the onset of shear failure and $\gamma \geq \gamma_{sh,f}$ the corresponding average shear strain in the critical shear length (Eq. 1), a a constant affecting the average slope and c the curvature of the descending branch curve. However, no strong correlation emerged between the geometric and loading parameters of specimens and the curvature of the curve. Therefore, the non-linear curve concept was no further pursued. A noteworthy finding, nonetheless, was that shear critical specimens tended to have mostly convex post-peak responses, while flexure-shear critical specimens had a linear on average, with approximately equal number of convex and concave curve cases (Figure 8b).

Subsequently, modelling the descending branch with a linear segment was considered, taking into account its simplicity, its compatibility with the proposed shear model and its match with experimental results, the Coefficient of Determination (R^2) of fitting a least-squares line to the experimental post-peak response having an average value of 0.95 and a *CoV* of 7.4%.

The linear descending branch herein is defined by fitting a least-squares line starting from the onset of shear failure. Were it defined by a line connecting the onset of shear and axial failure instead (e.g. [24], [25]), the energy dissipated by an element could be significantly under- or overestimated. For instance, in the case of the convex curve of Figure 4b, this would lead to an overestimation of the dissipated energy. The opposite would happen in concave curves; the deviation would generally be larger the farther away from a linear descending branch a specimen's post-peak strength degradation is.

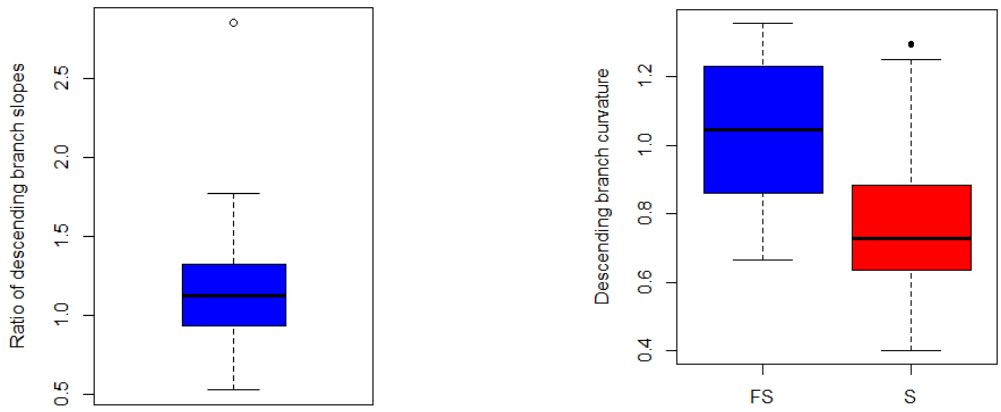

(a) (b)

Figure 8: Ratio of descending branch slopes in two "directions" of the response of the database specimens (a). Curvature of the descending branch (c) of the response of flexure-shear critical (FS) and shear critical (S) specimens of the database (b).

A bilinear curve with a horizontal branch representing residual strength, assumed by previous studies (e.g. [19], [23]), was judged to be a viable choice for less than 10% of all specimens in the database. This suggests either that practically no residual strength is developed in shear critical R/C members (at least those with the characteristics of this database), or that axial failure occurs in most specimens before they reach their residual capacity; hence, such an approach was no further pursued.

Nevertheless, a bilinear branch with two independent slopes was pursued, with the breaking point being at 50% strength degradation, as in Figure 1. This approach was believed to lead to a more

accurate representation of the post-peak descending branch overall, as it is much more flexible and can represent linear, convex and concave responses, observed experimentally (Figure 8b). Only specimens with at least 80% strength degradation were used to measure the value of the slope of the second segment of their post-peak response, hence only 37 specimens were taken into account in this case.

The proposed linear shear strength degradation relationship is the following:

$$\frac{V}{V_{\max}} = 1 - S_{pp} \times (\gamma - \gamma_{sh,f}) \quad (4)$$

where S_{pp} is a dimensionless parameter expressing the shear strength degradation normalised to V_{max} per unit of post-peak shear strain and $\gamma \geq \gamma_{sh,f}$ the corresponding average shear strain in the critical shear length (Eq. 1). The dimensionless slope value S_{pp} will have to be multiplied by a specimen's maximum shear strength and divided by its critical shear length to get the slope in units of force per length.

It has been pointed out (e.g. in FEMA P440A [40]) that in-cycle strength degradation should not be confounded with cyclic strength degradation; this has also been shown experimentally, for instance by observing the apparent difference in the descending branch slope of identical specimens that were cycled following different loading protocols [10]. Therefore, they should be, and have been herein, treated separately. Specimens with at least 30% degradation in their total shear strength being attributed to in-cycle degradation were termed "quasi-monotonic" (**QM**), i.e. it was assumed that their strength degradation was mainly due to in-cycle degradation mechanisms, while the rest were considered "cyclic specimens" (**CS**). The former amounted to a total of 30, the latter to 86, i.e. a total of 116 specimens in the database were available - hereafter called "all specimens" (**AS**).

- Empirical equations developed for **QM** will be more appropriate for modelling specimens with high in-cycle degradation due to the displacement history used (purely monotonic or cyclic with large displacement steps) or members of actual structures which are expected to exhibit very high in-cycle degradation, e.g. when subjected to near-field, pulse-like, ground motions.
- **CS** will be most appropriate for cyclic tests with loading protocols with more than one cycles at each displacement level and small displacement steps, i.e. the typical cyclic quasi-static symmetrical loading protocols.
- **AS** will be more appropriate for 'scenarios' wherein a mix of both types of strength degradation is expected, i.e. structures subjected to earthquakes, exhibiting both cyclic and in-cycle degradation.

Based on these datasets, several patterns emerged examining the correlation of the descending branch slope (in a V/V_{max} vs γ curve) with geometric, material and loading parameters (in Figure 9, the trends observed in the dataset **AS** are shown, being indicative of the other datasets, too):

- Higher axial load ratio increases the shear strength degradation rate, as has been often noted in similar studies (e.g. [9]).
- Increased longitudinal reinforcement leads to a decreased post-peak slope, mainly through the dowel action of the longitudinal bars, as well as carrying an (occasionally significant) part of the vertical load, hence reducing the damage inflicted on the crack interface during load reversals. It is noteworthy that the longitudinal reinforcement ratio divided by the ratio of the confined to the total cross-section area gives a better prediction than the unnormalised ratio, the latter being more common a variable in pre-peak models. This can be attributed to the fact that after the critical shear crack has formed at the onset of shear degradation, the effective concrete area is the confined one, as the unconfined cover concrete either has already spalled off within the member critical length or it does not actively contribute as resistance mechanism, due to substantial reduction in its strength.
- Higher transverse reinforcement is beneficial, as expected; the transverse steel bars crossing the critical crack are one of the main shear resistance mechanisms.
- The average diameter of longitudinal bars over the effective depth, $\Phi_{l,ave}/d$, seems to play an important role, too, decreasing the degradation rate as it increases.
- Aspect ratio was investigated, as it was considered important in a previous model (e.g. [41], but

was found not to hold very high predictive strength. This is attributed to the fact that the localisation of shear strains in the critical length was considered, hence eliminating the effect of aspect ratio, which is pronounced when taking into account the inter-storey drift ratio and disregarding shear failure localisation.

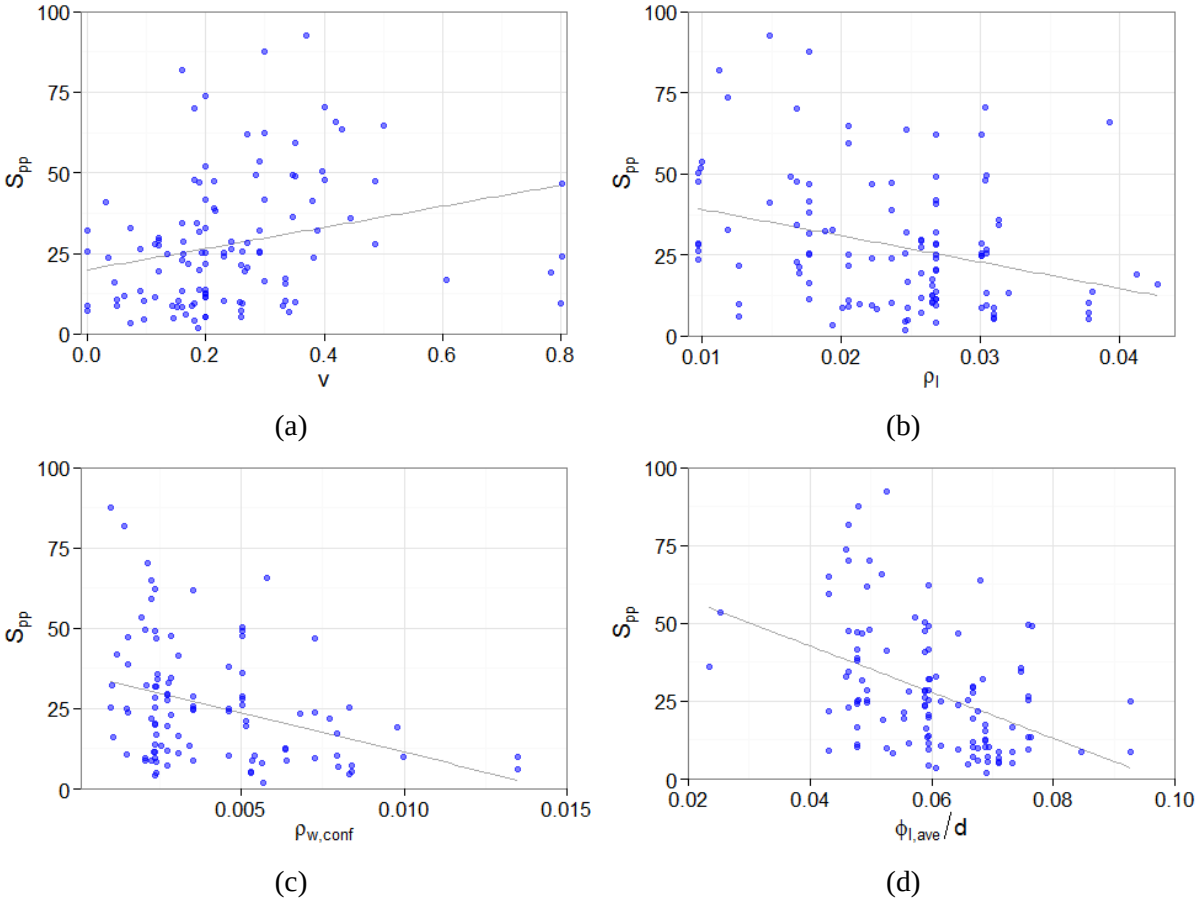

Figure 9: Correlation of slope of the linear post-peak branch of the **AS** dataset with axial load ratio (a), longitudinal reinforcement ratio (b), transverse reinforcement ratio normalised to confined concrete area (c), and average longitudinal bar diameter normalised to effective depth (d).

Based on these trends and significance tests of the predictor variables, various potential predictive relations were explored. The final expressions were developed through a step-wise predictor variable elimination procedure, 10-fold-cross-validation [38] and optimisation using the Levenberg-Marquardt nonlinear least-squares algorithm (e.g. [39]). For a linear post-peak branch, where the entire post-peak response is taken into account, the following expressions are proposed (for **QM**, **CS** and **AS** specimens, respectively):

$$S_{pp} = \frac{0.0134\left(v+0.05\right)^{0.533}}{\left(\rho_{w,conf}+0.0003\right)^{0.633}\left(\frac{\rho_l}{\alpha_{conf}}+0.7\right)^{15.4}} - 3.75 \geq 2 \tag{5}$$

$$S_{pp} = \frac{0.00302\left(v+0.3\right)^{0.839}}{\left(\rho_{w,conf}+0.0155\right)^{2.48}\left(L_s/d\text{-}0.9\right)^{0.159}} - 9.25 \geq 2 \tag{6}$$

$$S_{pp} = \frac{2.01\cdot10^{-6}\left(v+0.255\right)^{1.06}\left(\frac{\tau_{max}}{\sqrt{f_c}}\text{-}0.21\right)^{0.0528}}{\left(\rho_{w,conf}+0.0039\right)^{1.71}\left(L_s/d\text{-}0.9\right)^{0.207}\left(\rho_l+0.35\right)^{8.67}}+2.01\geq 2 \quad (7)$$

For the first segment of a bilinear post-peak branch, up to 50% loss of V_{max} (Fig. 1), the following expressions are proposed (for **QM**, **CS** and **AS** specimens, respectively):

$$S_{pp,1} = \frac{1.25\cdot10^{-4}\left(v_l\text{-}0.20\right)^{0.201}}{\left(\rho_{w,conf}+0.0075\right)^{2.8}\left(L_s/d-1.05\right)^{0.183}}-4.38\geq 2 \quad (8)$$

$$S_{pp,1} = \frac{0.8\left(v+0.145\right)^{0.23}}{\left(\rho_{w,conf}+0.0033\right)^{0.587}\left(L_s/d\text{-}0.408\right)^{0.25}\left[\frac{\rho_l}{\alpha_{conf}}\left(\frac{\Phi_{l,ave}}{d}\right)+0.0053\right]^{0.379}}-40.5\geq 2 \quad (9)$$

$$S_{pp,1} = \frac{2.65\cdot10^{-5}\left(v+0.0618\right)^{0.386}\left(\frac{\tau_{max}}{\sqrt{f_c}}\text{-}0.20\right)^{0.115}}{\left(\rho_{w,conf}+0.0077\right)^{2.42}\left(L_s/d\text{-}0.90\right)^{0.207}\left(\rho_l+0.208\right)^{2.61}}-5.52\geq 2 \quad (10)$$

For the second segment of a bilinear post-peak branch, after 50% loss of V_{max} (Fig. 1), the following expressions are proposed (for **QM**, **CS** and **AS** specimens, respectively):

$$S_{pp,2} = 40.3\left(v_l-0.0756\right)^{0.538}\left(s/d+0.425\right)^{1.26}\text{-}8.2\geq 2 \quad (11)$$

$$S_{pp,2} = \frac{232\left(v_l-0.115\right)^{0.0236}\left(s/d+0.15\right)^{0.033}}{\left(\rho_{w,conf}+0.125\right)^{1.05}\left(\frac{\rho_l}{\alpha_{conf}}+1.76\right)^{2.77}}-363\geq 2 \quad (12)$$

$$S_{pp,2} = \frac{0.206\left(v_l\text{-}0.15\right)^{0.16}\left(s/d+0.0003\right)^{0.393}}{\left(\rho_{w,conf}+0.0018\right)^{0.149}\left(\frac{\rho_l}{\alpha_{conf}}+0.22\right)^{3.51}}-15.15\geq 2 \quad (13)$$

Table 2: Summary of the main statistics of accuracy and variation of the relationships developed (Eq. 5-13).

Eq.	**(5)**	**(6)**	**(7)**	**(8)**	**(9)**	**(10)**	**(11)**	**(12)**	**(13)**
R^2	0.80	0.45	0.54	0.64	0.51	0.58	0.73	0.54	0.51
mean	1.00	1.04	1.01	1.00	1.02	1.02	1.00	0.99	1.01
median	0.97	0. 95	0.91	0.93	0.94	0.95	0.96	0.83	0.90
***CoV* (%)**	40.3	57.1	49.6	45.0	47.8	53.5	31.2	63.1	61.3

Table 2 summarises the accuracy and variation statistics of the above presented relations (mean and median refer to the ratio of experimental to predicted values). Table 3 includes the size of the datasets used for the derivation of each expression as well as the ranges of the main parameters, inside which these models are valid. Regarding the parameters used, ρ_l is the longitudinal reinforcement ratio,

introduced with its actual value (not in %); α_{conf} is the ratio of the confined to the total cross-section area; $\tau_{max} / \sqrt{f_c}$ is the maximum average shear stress normalised to the square root of the concrete compressive strength; v_l is the longitudinal reinforcement axial load ratio, i.e. the axial load divided by the axial capacity of the longitudinal rebars; L_s/d is the member aspect ratio; $\Phi_{l,ave}/d$ is the average diameter of longitudinal bars normalised to the effective depth (to avoid scaling issues); s/d is the spacing of stirrups over the effective depth of the cross-section. The lower threshold used in all equations is the value 4, corresponding to the lowest slope value encountered in the database.

Scatter plots of experimental against predicted values of the descending branch are indicatively presented for some equations (Eq. 7, 9 and 11) in Figure 10. The scatter in some models is also influenced by the very high uncertainty inherent in post-peak phenomena, for instance, the history of demands and the randomness of the succession of degradation phenomena taking place at a lower level. This is obvious also in similar existing models that exhibit high variation (e.g. R^2 of 0.6 in [30]). As expected, the models for **QM** specimens have lower variation compared to **CS** and **AS** in every case; this is due to the fact that in-cycle degradation in these specimens is captured via these models, while the slopes of CS specimens are substantially affected by the displacement pattern used for each test, leading to potentially lower or higher cyclic strength degradation, thus producing extra uncertainty.

Table 3: Datasets and minimum and maximum limits of main design parameters defining the range of application of the proposed relationships.

Dataset / No. of specimens	v	$\rho_{w,conf}$ **%**	$\Phi_{l,ave}/d$ **[×10^{-3}]**	ρ_l/α_{conf} **%**	f_{yl} **[MPa]**	f_{yw} **[MPa]**	f_c **[MPa]**	L_s/d
Linear branch and first segment of bilinear branch (at least 30% degradation)								
QM / 30	[0.07, 0.60]	[0.00, 0.85]	[45, 75]	[1.50, 5.45]	[330, 700]	[250, 590]	[13.5, 86]	[1.1, 3.8]
CS / 86	[0.00, 0.80]	[0.00, 1.60]	[25, 140]	[0.20, 6.50]	[330, 540]	[295, 560]	[13.5, 86]	[0.9, 4.3]
AS / 116	[0.00, 0.80]	[0.00, 1.60]	[25, 140]	[0.20, 6.50]	[330, 700]	[250, 590]	[13.5, 86]	[0.9, 4.3]
Second segment of bilinear branch (at least 80% strength degradation)								
QM / 16	[0.15, 0.30]	[0.12, 0.85]	[46, 75]	[2.20, 5.45]	[330, 550]	[355, 475]	[22, 31]	[1.1, 3.8]
CS / 21	[0.05, 0.40]	[0.08, 0.56]	[45, 75]	[1.65, 4.85]	[340, 460]	[290, 475]	[18, 32.5]	[1.1, 3.8]
AS / 37	[0.05, 0.40]	[0.08, 0. 85]	[45, 75]	[1. 65, 5.45]	[330, 550]	[290, 475]	[18, 32.5]	[1.1, 3.8]

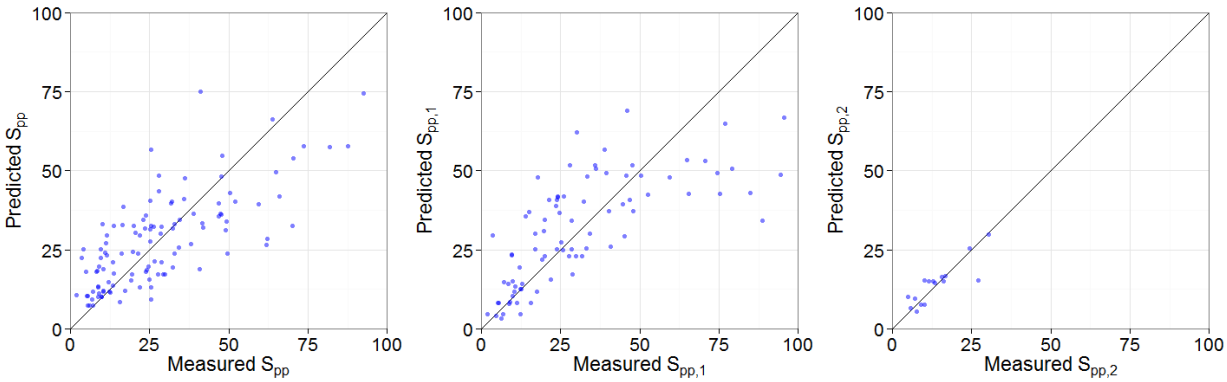

Figure 10: Values of post-peak descending branch slopes (dimensionless) measured experimentally (horizontal axes) against the ones predicted (vertical axes) using Eq. 7, 9 and 11 (from left to right).

In Figure 11, the values of the descending branch slope predicted by Eq. 5 are plotted against the longitudinal reinforcement ratio, for different transverse reinforcement ratios, for a low and a high axial load ratio. It is obvious that the higher the axial load and the lower the reinforcement of the

member, the steeper the slope of the descending branch is going to be, i.e. the higher the strength degradation after the onset of shear failure. For parameter values representative of common structures (i.e. $0.2 \leq v \leq 0.3$, $1.5 \leq \rho_l \leq 3.5$ (%) and $0.2 \leq \rho_w \leq 0.6$ (%)), the slope would have values between 10 and 40 (this is unitless, as it is multiplied by the maximum strength to get the degradation of strength per unit of shear distortion, see Eq. 4).

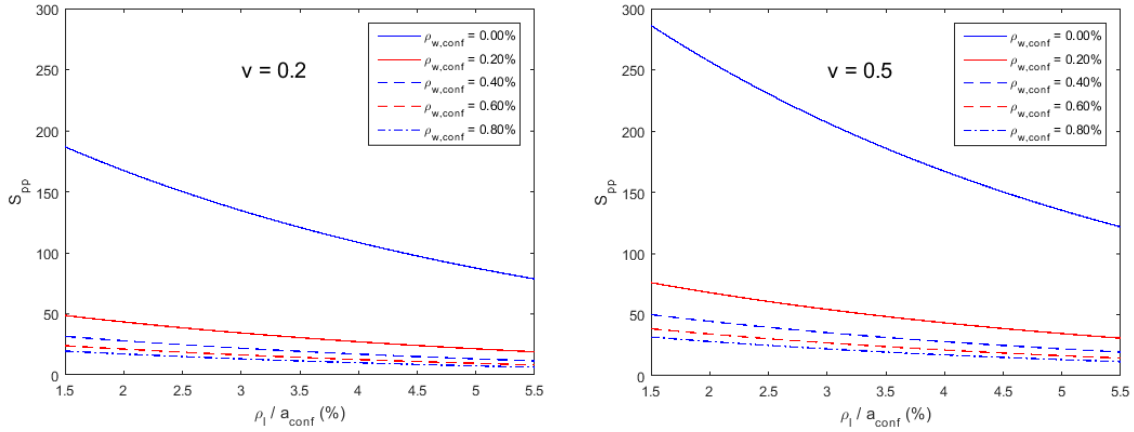

(a) (b)

Figure 11: Descending branch slope (S_{pp}) predicted by Eq. 5 along the range of potential longitudinal reinforcement ratios over relative confined concrete area, for different transverse reinforcement ratios over confined concrete area, for axial load ratios of 0.2 (a) and 0.5 (b).

3.4 Onset of axial failure

The axial load resistance degrades with lateral displacement reversals, due to gradual disintegration of the confined concrete core [1]; the onset of axial failure is defined at the point where axial load resistance and demand become equal, whereupon sudden decrease of axial load and increase of axial shortening take place. This constitutes a vital turning point in the non-linear response of the entire structure, since it signals the initiation of a process of loss of an individual vertical R/C element's axial load support (i.e. of its bearing capacity) simultaneously with the redistribution of vertical loads to its neighbouring members, potentially initiating vertical progressive collapse. A subset of specimens of the database has sustained such failure; this was determined based either on the provided axial hysteretic response (i.e. occurrence of high sudden axial shortening and/or sudden loss of axial capacity) and/or on the explicit report of axial failure of a column by the respective authors.

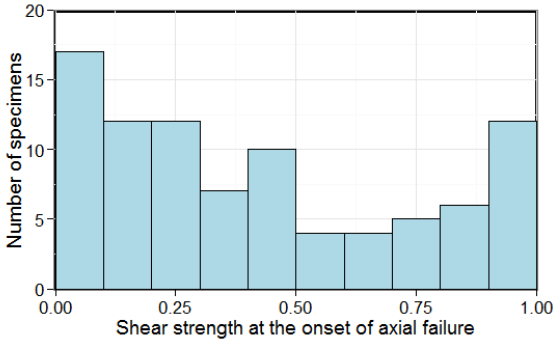

Figure 12: Residual shear strength normalised to the maximum shear strength at the onset of axial failure for the specimens of the compiled database.

It has long been claimed, based on limited amount of experimental data (e.g. [11]), that the onset of axial failure occurs when shear strength degrades to zero (or becomes negligible); several post-peak models have been based on this assumption (e.g. [24], [25]). Nonetheless, experimental evidence

shows that this cannot be taken for granted in all specimens. In fact, for many of them it is considerably misleading as shown in Figure 12, where the shear strength at the onset of axial failure is shown for the specimens that have sustained axial failure in this database; it is normalised by the respective strength at the onset of shear failure, to get the relative residual lateral strength. The ostensibly unrealistic values equal to or near 1.00 are in fact due to the specimens having undergone simultaneous shear and axial failure. Apparently, the shear strength of only a small fraction of the specimens has degraded to negligible values (10% or even 20%) of the maximum strength. Consequently, the assumption of zero strength at the onset of axial failure is certainly not experimentally sound; adopting it could potentially lead to high discrepancies i.e. much steeper descending branches and consequent great underestimation of the energy dissipation capacity, especially in cases where axial failure initiates before significant shear strength degradation.

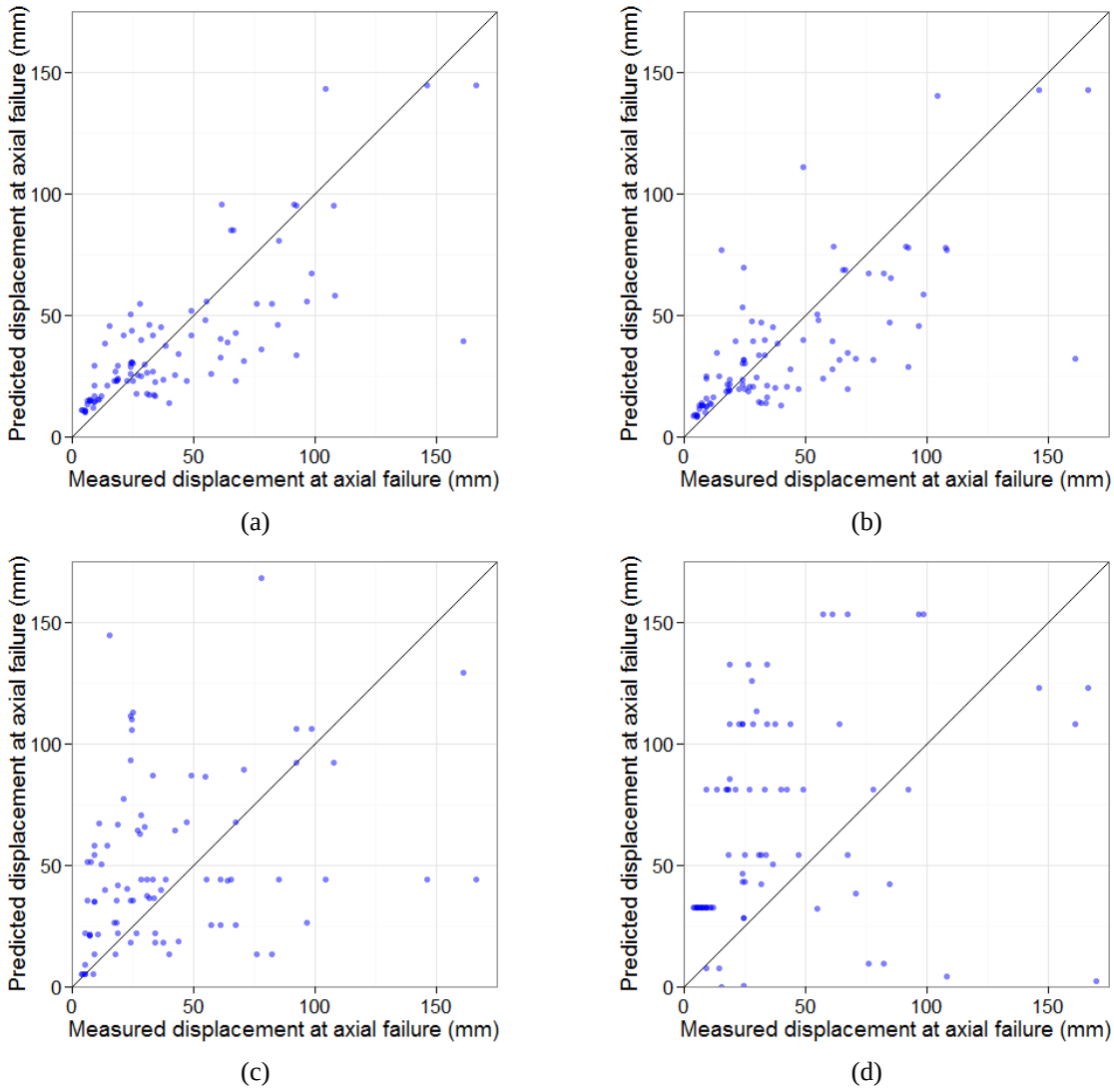

Figure 13: Existing predictive relations for the lateral displacement at the onset of axial failure (vertical axis) applied in this database, against measured displacements (horizontal axis). Elwood & Moehle [13] (a), Zhu *et al.* [42] (b), Yoshimura [43] (c), and Ousalem *et al.* [10] (d).

Therefore, a deformation-based criterion is sought, instead. Existing models predicting the lateral displacement at the onset of axial failure were applied in this extensive dataset of 89 specimens having sustained axial failure, to find the most accurate one to employ. The predictive ability of these models is shown in Figure 13. The models by Ousalem *et al.* [10] and Yoshimura [43] seem to exhibit very high scatter, in some cases overestimating and in other cases underestimating significantly the lateral displacement. Elwood & Moehle, and Zhu *et al.* models [13], [42] seem to capture the displacements

on average better than the other models, but they also exhibit high scatter (mean 1.18 and 1.28, and *CoV* 73.4% and 75.7%, respectively). Most of these models ([10], [13], [42]) have been calibrated only to flexure-shear critical specimens and they are all based on rather limited datasets.

To improve the accuracy of the predictions, a new deformation-based empirical model is developed in this study to capture the onset of axial failure of an R/C element. In line with the local shear hysteretic model described in the previous sections (Figure 1), the deformation parameter used is the average post-peak shear strain $\gamma_{t,pp}$ in the critical shear length L_{cr} at onset of axial failure determined by the following equation:

$$\gamma_{t,pp} = \frac{\delta_{ax,f} - \delta_{sh,f}}{L_{cr}} \tag{14}$$

where $\delta_{ax,f}$ is the lateral displacement at the onset of axial failure, and $\delta_{sh,f}$ is the lateral displacement at the onset of shear failure.

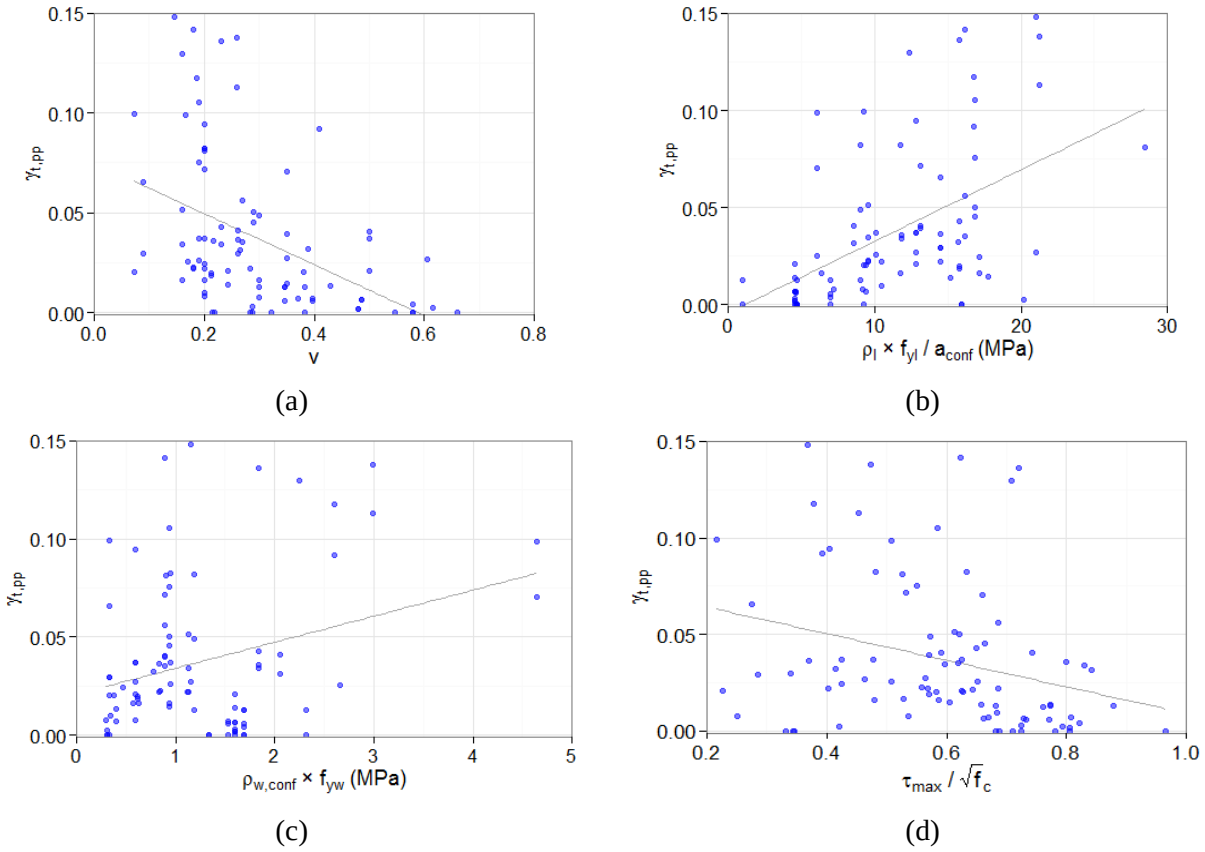

Figure 14: Correlation of total post-peak shear strain at the onset of axial failure ($\gamma_{t,pp}$) with axial load ratio (a), longitudinal reinforcement ratio divided by the percentage of confined area and multiplied by its yield strength (b), transverse reinforcement ratio multiplied by its yield strength (c) and maximum average shear stress ratio (d).

Based on this dataset, the following patterns emerged, examining the correlation of the local post-peak average shear strain with design, material and loading parameters (Figure 14):

- Axial load ratio is a pivotal parameter, associated with decrease in member deformability, as has been noted in many similar studies (e.g. [9], [13]).
- Higher longitudinal reinforcement is beneficial, increasing the post-peak deformability, as also observed in previous studies (e.g. [11]). Longitudinal bars take up part of the axial load, partially relieving the confined concrete core from damage inflicted during the displacement reversals. Also, it allows for redistribution of a higher percentage of the axial load from concrete to steel in later stages.
- As expected, transverse reinforcement is beneficial, a fact underlined repeatedly in the past (e.g. [9], [13]). It confines the concrete core, allowing for higher bearing capacity and takes up a

significant part of the shear force, decreasing the shear strength degradation of the member and the damage inflicted to the core along the shear failure plane.

- The higher the maximum average shear stress at the point of maximum lateral loading, the lower the achieved deformation at the onset of axial failure.

There are other influential factors, too, e.g. load path and failure type. As noted in the past (e.g. [1]), monotonic response leads to higher deformability than cyclic. Flexure-shear critical specimens (FS) seem to exhibit higher deformability on average, when contrasted with shear-critical ones (S).

Based on these trends and significance tests of the predictor variables, various potential predictive relationships were explored. The final expression was developed through a step-wise predictor variable elimination procedure, 10-fold-cross-validation [38] and optimisation using the Levenberg-Marquardt nonlinear least-squares algorithm (e.g. [39]):

$$\gamma_{t,pp} = \frac{0.0193\left(\rho_{w,conf} - 0.00074\right)^{0.422}\left(\frac{\rho_l f_{yl}}{\alpha_{conf}} - 0.985\right)^{0.899}}{\left(\nu + 0.504\right)^{3.85}\left(\tau_{ave,max}/\sqrt{f_c} - 0.215\right)^{0.162}} - 5\cdot 10^{-4} \geq 0 \quad (15)$$

where ρ_l, $\rho_{w,conf}$ are introduced with their actual value (not in %). Eq. 15 yields a mean experimental-to-predicted value of 1.01, a median of 0.77, a *CoV* of 84.0% and an R^2 of 0.69, including all specimens. However, the inclusion of the specimens having a very low value of deformation (close to zero) results in extreme values; excluding the ones equal to or lower than 0.01, one gets the following values instead: 1.01, 0.85, 68.7% and 0.63. Despite the fact that the experimental-to-predicted ratios statistics are worse for $\gamma_{t,pp}$ predictions lower than 0.01, this is not considered as a serious problem because in terms of absolute values the errors are small. This is also verified by the high R^2 value achieved in both cases. The predictive ability of the expression, including all specimens, can also be seen in Figure 15. Its application is valid in the following range of parameters: $0.07 < \nu < 0.66$, $0.08 < \rho_w \leq 1.35$ (%), $0.15 < \rho_l \leq 3.8$ (%), $331 \leq f_{yl} \leq 700$ (MPa), $303 \leq f_{yw} \leq 587$ (MPa), $13.5 \leq f_c \leq 33.6$ (MPa), $1 < L_s/d \leq 4.25$.

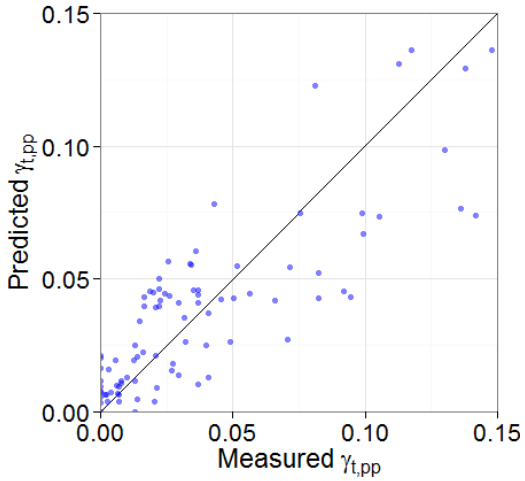

Figure 15: Measured total post-peak shear strain at the onset of axial failure against the predicted one using Eq. 15.

In Figure 16, the values of the total post-peak shear strain ($\gamma_{t,pp}$) predicted by Eq. 15 are plotted against the transverse reinforcement ratio normalised to the confined concrete volume ($\rho_{w,conf}$), for different longitudinal reinforcement indices ($\rho_l/\alpha_{conf,\%} \times f_{yl}$), for axial load ratios (ν_l) of 0.25 and 0.5 and for a maximum shear stress ratio ($\tau_{max}/\sqrt{f_c}$) of 0.25 and 0.75. The aspect ratio was set at the median value of the dataset (L_s/d = 1.65), as this parameter was found not to influence the result as much as the others. It is obvious that the higher the axial and shear loading and the lower the transverse and longitudinal reinforcement of the member, the lower its deformability, i.e. the lower the total post-

peak shear strain at the onset of axial failure. For values of parameters representative of common structures (i.e. $0.2 \leq \nu \leq 0.3$, $1.5 \leq \rho_l \leq 3.5$ (%) and $0.2 \leq \rho_w \leq 0.6$ (%)), the post-peak shear strain would have values between 5% and 20%.

With the post-peak parameters calculated using the empirical equations proposed in this section, the hysteretic shear model described in section 2 can be defined. The implementation of the model in a beam-column element with distributed shear (and flexural) flexibility, which accounts for all deformation types of sub-standard R/C members, will be presented in a forthcoming paper.

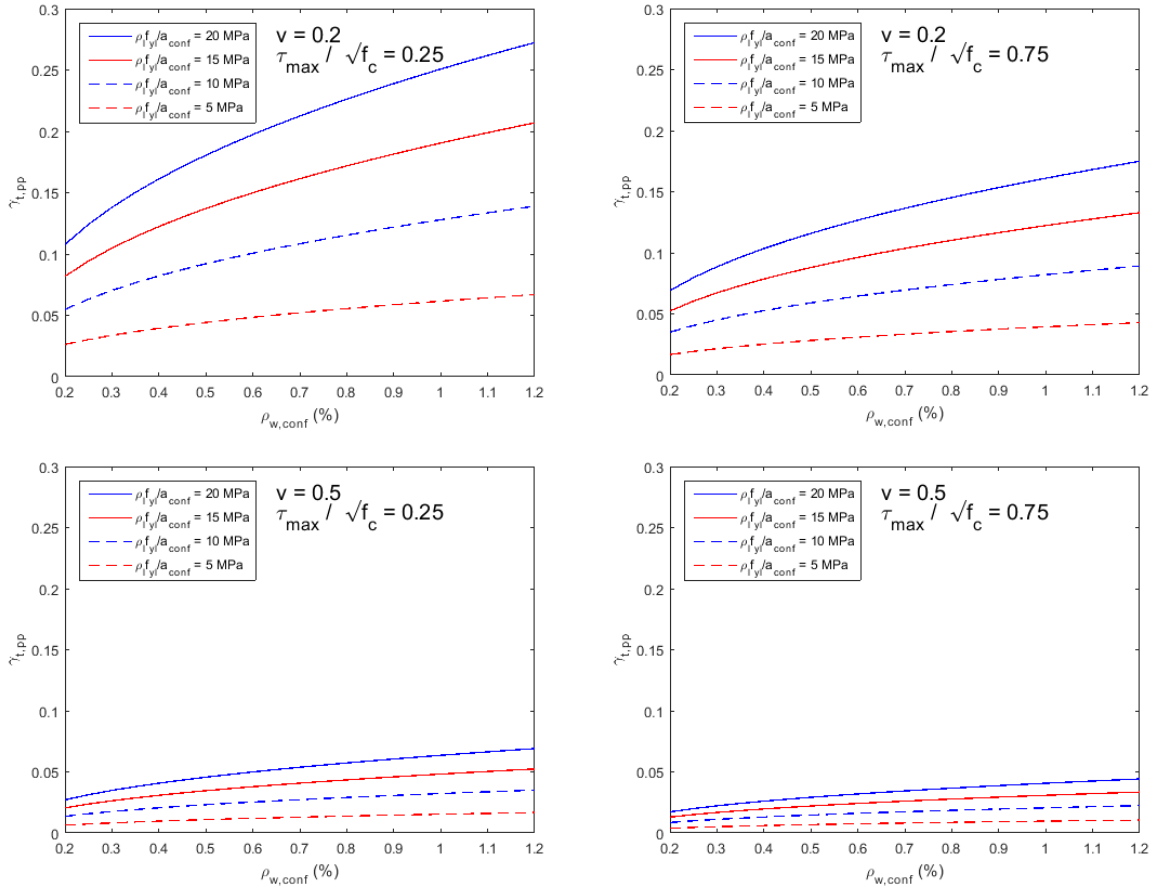

Figure 16: Total post-peak shear strain predicted by Eq. 15 along the range of longitudinal reinforcement ratios multiplied by the yield strength (over confined area) and transverse reinforcement ratios (over confined concrete area), for axial load ratios of 0.25 (top) and 0.5 (bottom) and maximum shear stress ratio of 0.25 (left) and 0.75 (right).

4. CONCLUSIONS

A hysteretic model was put forward herein, determining the pre-peak as well as post-peak shear response of an R/C member. It is a local hysteretic shear model, in that it accounts for the localisation of shear strains, after the onset of shear failure, in a critical length defined by the diagonal failure planes, namely shear failure localisation. Its backbone envelope and hysteresis rules are presented, with emphasis on the model's post-peak domain, including issues pertinent to the cyclic and in-cycle strength degradation as well as pinching, unloading and reloading stiffness deterioration.

Furthermore, to provide reliable predictions of the local post-peak response of shear critical R/C elements, a database of experimental results for shear and flexure-shear critical R/C columns – the largest of its kind – is compiled and empirical expressions for the key parameters of the backbone local post-peak shear response are developed. These parameters are: (i) the critical shear crack angle, hence the critical length wherein damage concentrates after the onset of shear failure, (ii) the descending branch of the curve after the onset of shear failure, for which separate expressions are proposed for a linear and a bilinear curve with breaking point at 50% shear strength degradation with

independent slopes, as well as separate cases for monotonic and cyclic loading, and (iii) the deformation at the onset of axial failure.

Noteworthy findings, additional to the expressions per se, are:

- High axial load ratio, low transverse reinforcement ratio and pure shear failure were shown to result in steeper critical shear crack angles. For common structures, angles of approximately 25°-30° and 30°-35° (with respect to the column longitudinal axis) would be expected for shear and flexure-shear critical specimens, respectively.
- Initiation of shear failure in one direction has been shown not to affect considerably the degradation rate in the other direction, i.e. their descending branch slopes tend to be similar.
- The data suggests either that practically no residual strength is developed in shear critical R/C members (at least those with the characteristics of this database) or that axial failure occurs in most specimens before they reach their residual capacity.
- Higher transverse and longitudinal reinforcement content, as well as lower axial load are generally shown to reduce the post-peak shear strength degradation rate, i.e. milder descending branch slope, and lead to higher deformability. For common structures, the total post-peak shear strain would have values between 5% and 20%.
- Shear strength has been typically considered zero at the onset of axial failure. It has been shown herein that this is not a valid assumption; its adoption could lead to high discrepancies by producing much steeper descending branches and great underestimation of the energy dissipation capacity, especially in cases where axial failure initiates before significant shear strength degradation.

The local hysteretic shear model will be incorporated in a computationally efficient member-type model for the full-range response of substandard elements in a forthcoming paper, with a view to accurately capturing the response of shear-deficient R/C elements and structures. It is based on local shear deformations, rather than inter-storey displacements, thus more objectively accounting for the interaction of inelastic flexural and shear deformations, including the gradual decrease of an element's shear resistance, and more reliably predicting the location and extent of shear damage, without relying on assumptions about the bending moment distribution (which generally changes during seismic loading).

5. ACKNOWLEDGEMENTS

This research study was conducted as part of the doctoral degree of the first author funded by City, University of London and the A. G. Leventis Foundation.

6. REFERENCES

1. Sezen H, Moehle JP. Seismic tests of concrete columns with light transverse reinforcement. *ACI Structural Journal* 2006, **103**(6): 842–849.
2. Ghannoum WM, Moehle JP, Bozorgnia Y. Analytical collapse study of lightly confined reinforced concrete frames subjected to Northridge earthquake ground motions, *Journal of Earthquake Engineering* 2008, **12**(7): 1105-1119. DOI 10.1080/13632460802003165
3. Mergos PE, Kappos AJ. A gradual spread inelasticity model for R/C beam–columns, accounting for flexure, shear and anchorage slip. *Engineering Structures* 2012, **44**: 94–106. DOI: 10.1016/j.engstruct.2012.05.035
4. Ozcebe G, Saatcioglu M. Hysteretic shear model for reinforced concrete members. *Journal of structural engineering* 1989, **115**(1): 132–148. DOI: 10.1061/(ASCE)0733-9445(1989)115:1(132)
5. Lee JY, Watanabe F. Predicting the longitudinal axial strain in the plastic hinge regions of reinforced concrete beams subjected to reversed cyclic loading. *Engineering Structures* 2003, **25**(7):927–939.DOI: 10.1016/S0141-0296(03)00026-9
6. Priestley NMJ, Verma R, Xiao Y. Seismic shear strength of reinforced concrete columns. *Journal of Structural Engineering* 1994, **120**(8): 2310–2329. DOI: 10.1061/(ASCE)0733-9445(1994)120:8(2310)
7. Sezen H, Moehle JP. Shear strength model for lightly reinforced concrete columns. *Journal of Structural Engineering* 2004, **130**(11): 1692–1703. DOI: 10.1061/(ASCE)0733-9445(2004)130:11(1692)

8. Biskinis DE, Roupakias GK, Fardis MN, Degradation of shear strength of reinforced concrete members with inelastic cyclic displacements. *ACI Structural Journal* 2004, **101**(6): 773–783.
9. Ousalem H, Kabeyasawa T, Tasai A, Ohsugi Y. Experimental study on seismic behavior of reinforced concrete columns under constant and variable axial loadings. *Proceedings of the Japan Concrete Institute* 2002, **24**(2): 229-234.
10. Ousalem H, Kabeyasawa T, Tasai A. Evaluation of ultimate deformation capacity at axial load collapse of reinforced concrete columns. *13th World Conference on Earthquake Engineering* 2004, Paper No. 370.
11. Yoshimura M, Nakamura T. Axial collapse of reinforced concrete short columns, *The 4th US-Japan Workshop on Performance-Based Earthquake Engineering Methodology for Reinforced Concrete Building Structures*, *PEER 2002/21* 2002: 187–198.
12. Henkhaus K, Pujol S, Ramirez J. Axial failure of reinforced concrete columns damaged by shear reversals. *Journal of Structural Engineering* 2013, **139**(7): 1172–1180. DOI: 10.1061/(ASCE)ST.1943-541X.0000673
13. Elwood KJ, Moehle JP. Axial capacity model for shear-damaged columns. *ACI Structural Journal* 2005,**102**(4):578–587.
14. Ousalem H, Kabeyasawa T. Drift at axial load failure under cracked-region-sway mechanism for reinforced concrete columns. *Proceedings of the Japan Concrete Institute* 2006, **28**(2): 223-228.
15. Vecchio FJ, Collins MP. The modified compression-field theory for reinforced concrete elements subjected to shear. *ACI Journal Proceedings* 1986, **83**(2): 219–231.
16. Hsu TTC. Softened truss model theory for shear and torsion. *ACI Structural Journal* 1988, 85(6): 624-635.
17. Hsu TTC, Zhu RRH. Softened membrane model for reinforced concrete elements in shear. *ACI Structural Journal* 2002, **99**(4): 460 – 469.
18. Mostafaei H, Kabeyasawa T. Axial-shear-flexure interaction approach for reinforced concrete columns. *ACI Structural Journal* 2007, **104**(2): 218–226.
19. Pincheira JA, Dotiwala FS, D'Souza JT. Seismic analysis of older reinforced concrete columns. *Earthquake Spectra* 1999, **15**(2): 245–272. DOI: 10.1193/1.1586040
20. Lee DH, Elnashai AS. Seismic analysis of RC bridge columns with flexure-shear interaction**.** *Journal of Structural Engineering* 2001, **127**(5): 546–553. DOI: 10.1061/(ASCE)0733-9445(2001)127:5(546)
21. Sezen H, Chowdhury T. Hysteretic model for reinforced concrete columns including the effect of shear and axial load failure. *Journal of Structural Engineering* 2009, 135(2): 139–146. DOI: 10.1061/(ASCE)0733-9445(2009)135:2(139)
22. Baradaran Shoraka M, Elwood KJ. Mechanical model for non ductile reinforced concrete columns. *Journal of Earthquake Engineering* 2013, 17(7): 937–957. DOI: 10.1080/13632469.2013.794718
23. LeBorgne MR, Ghannoum WM. Analytical element for simulating lateral-strength degradation in reinforced concrete columns and other frame members. *Journal of Structural Engineering* 2014, **140**(7): 04014038. DOI: 10.1061/(ASCE)ST.1943-541X.0000925
24. Elwood KJ. Modelling failures in existing reinforced concrete columns. *Canadian Journal of Civil Engineering* 2004, **31**(5): 846–859. DOI: 10.1139/L04-040
25. Sezen H. Shear deformation model for reinforced concrete columns. *Structural Engineering and Mechanics* 2008, **28**(1): 39–52.
26. Kato D, Zhuzhen LI, Yatsutsuka T, Nakamura Y. Axial load capacity of RC columns with various reinforcing details and concrete strength. *1st European Conference on Earthquake Engineering and Seismology* 2006: 1–10, Paper No. 347.
27. Shirai N, Lejano BA, Adachi H, Nakanishi M. Flexure and shear behavior of high strength reinforced concrete column subjected to high and fluctuating axial load. *11th World Conference on Earthquake Engineering* 1996, Paper No. 1199.
28. Wibowo A. Drift capacity of lightly reinforced soft storey structures**.** *Jurnal Rekayasa Sipil* 2013, **7**(2): 166-177.
29. Mergos PE, Kappos AJ. A distributed shear and flexural flexibility model with shear–flexure interaction for R/C members subjected to seismic loading. *Earthquake Engineering & Structural Dynamics* 2008, 37(12): 1349–1370. DOI: 10.1002/eqe.812
30. LeBorgne MR, Ghannoum WM. Calibrated analytical element for lateral-strength degradation of reinforced concrete columns. *Engineering Structures* 2014, **81**: 35–48. DOI: 10.1016/j.engstruct.2014.09.030
31. Fardis MN, Biskinis D, Grammatikou S. RC Members in Cyclic Loading: Strength, Deformation Capacity, Failure Modes, *8th International Conference on Analytical Models and New Concepts in Concrete and Masonry Structures* 2014.
32. Comité Européen de Normalisation (CEN). Eurocode 8. Design of structures for earthquake resistance. Part 3: Assessment and retrofitting of buildings, *EN 1998-3* 2005.
33. Biskinis DE, Fardis MN. Stiffness and cyclic deformation capacity of circular RC columns with or without lap-splices and FRP wrapping. *Bulletin of Earthquake Engineering* 2013, **11**(5): 1447–1466. DOI: 10.1007/s10518-013-9442-7
34. Zimos, DK. Modelling the Post-Peak Response of Existing Reinforced Concrete Frame Structures Subjected to Seismic Loading. *PhD Thesis*. City, University of London, United Kingdom, 2017.
35. Umehara H, Jirsa J. Shear strength and deterioration of short reinforced concrete columns under cyclic deformations, *PMFSEL REPORT No. 82-3* 1982, The University of Texas at Austin.
36. Kim J, Mander J. Truss modeling of reinforced concrete shear-flexure behavior, *Technical Report MCEER-99-0005* 1999, Buffalo, New York.
37. Zimos DK, Mergos PE, Kappos AJ. Shear hysteresis model for reinforced concrete elements including the post-peak range, *5th ECCOMAS Thematic Conference on Computational Methods in Structural Dynamics and Earthquake Engineering, COMPDYN* 2015: 2640-2658. DOI: 10.7712/120115.3565.1184
38. Refaeilzadeh P, Tang L, Liu H. Cross-Validation, *Encyclopedia of Database Systems*. Springer US, 2009; 532-538. DOI: 10.1007/978-0-387-39940-9_565
39. Levenberg K. A method for the solution of certain non-linear problems in least squares. *Quarterly of Applied Mathematics* 1944, **2**(2): 164-168.
40. Applied Technology Council (ATC). Effects of strength and stiffness degradation on seismic response. *FEMA P440A* 2009, Washington, D.C.

41. Wibowo A, Wilson JL, Lam NTK, Gad EF. Drift performance of lightly reinforced concrete columns. *Engineering Structures* 2014, **59**: 522–535. DOI: 10.1016/j.engstruct.2013.11.016
42. Zhu L, Elwood KJ, Haukaas T. Classification and seismic safety evaluation of existing reinforced concrete columns. *Journal of Structural Engineering* 2007, **133**(9): 1316–1330. DOI: 10.1061/(ASCE)0733-9445(2007)133:9(1316)
43. Yoshimura M. Formulation of post-peak behavior of old reinforced concrete columns until collapse. *The 14th World Conference Earthquake Engineering* 2008.